

Spectral Properties of Effective Dynamics from Conditional Expectations

Feliks Nüske^{1,4}, Péter Koltai², Lorenzo Boninsegna^{3,4}, and Cecilia Clementi⁴

¹Institute of Mathematics, Universität Paderborn, Germany

²Department of Mathematics and Computer Science, Freie Universität Berlin, Germany

³University of California Los Angeles, Institute for Quantitative and Computational Biosciences
and Department of Microbiology, Immunology and Molecular Genetics

⁴Center for Theoretical Biological Physics and Department of Chemistry, Rice University, USA

Abstract

The reduction of high-dimensional systems to effective models on a smaller set of variables is an essential task in many areas of science. For stochastic dynamics governed by diffusion processes, a general procedure to find effective equations has recently been suggested in *Legoll and Lelièvre, Nonlinearity, 2010*. In this study, we investigate the approximation of slowly varying modes by the effective dynamics, which are associated to low-lying eigenvalues of the associated generator. Slowly varying variables are of particular interest in a variety of research fields, including molecular simulation. We prove a new relative error bound for these eigenvalues in the reversible setting. Moreover, we discuss the applicability of these results to Langevin dynamics, which is a highly popular model in molecular dynamics. We illustrate our findings on several benchmark systems. These examples provide further insights about parameter estimation for the effective dynamics.

1. Introduction

The description of high-dimensional dynamical systems by a reduced set of variables, usually referred to as *coarse graining* or *model reduction*, is of tremendous importance across many different fields of research. Examples range from finance to climate modeling to molecular biology. Two of the central reasons for the importance of coarse graining are that, firstly, analysis or numerical simulation of high-dimensional systems is often challenging or simply infeasible, and secondly, not all detailed features of the full system are needed in order to answer questions of scientific interest. Typical challenges arising along the search for a coarse grained model are 1) which properties of the high-dimensional system are important, and which ones are not, 2) what constitutes a good set of reduced variables (also called

Email: feliks.nueske@uni-paderborn.de

collective variables or *reaction coordinates* in some contexts), and 3) what is a suitable equation to define the low-dimensional description of the system, often called an *effective dynamics*.

From the huge body of literature on the subject, we mention in particular the Mori–Zwanzig formalism [1, 2, 3, 4, 5] as well as the framework of averaging and homogenization for systems with explicit multiscale structure [6, 7]. Within the field of molecular simulation, for which we consider several examples in this manuscript, Refs. [8, 9, 10, 11, 12, 13] present important contributions to this line of research. Yet another approach is based on conditioning along level sets of the coarse graining map [14, 15, 16]. For a detailed theoretical analysis of the method, please see [15, 17, 18, 19, 20].

An equally important issue is the data-driven inference of the parameters of the effective equations once a coarse graining scheme has been selected. A multitude of methods for accomplishing this goal have been developed, please see Ref. [21] for an overview. Spectral methods have been considered in [22, 23], while particular attention to the choice of time window has been paid in [24, 7]. Here, we will focus on properties of simple Kramers–Moyal type estimators [25], please see also the recent study [26] by some of the authors.

In many physical systems, there is a separation of timescales between slow relaxation processes and quickly equilibrating modes. This separation is reflected by a spectral gap for the system’s infinitesimal generator, or for its associated semigroup of Koopman operators. Therefore, we study the perturbation of these dominant eigenvalues if a high-dimensional dynamical system is reduced via the conditioning approach mentioned above. We emphasize that the results of this paper are not limited to systems with explicit multiscale structure as in [6]. The contributions of this study are as follows:

- For reversible systems with invariant measure μ , we provide a new relative error bound of the dominant generator eigenvalues in terms of the H_μ^1 -approximation error for the corresponding eigenfunctions. The relative error is a more practical error measure for small eigenvalues than the absolute error considered in [18]. Also, our new bound is less restrictive than the one obtained therein.
- We conjecture that dominant eigenvalues of the generator are also preserved if the parameters of the effective dynamics are estimated by Kramers–Moyal type estimators using a large time window. This hypothesis is backed up by numerical examples, using both toy systems as well as benchmark data sets of molecular dynamics simulations.
- We discuss the applicability of these results to (underdamped) Langevin dynamics if these are projected onto a transformation of their positional variables. While conditioning leads to meaningless dynamics in this case, we show that, if again a large time window is used for Kramers–Moyal type estimators, we recover the corresponding parameters of the overdamped process in the high-friction regime. In combination with the hypothesis stated above, this enables us to perform a meaningful model reduction even for underdamped Langevin dynamics.

The rest of this paper is organized as follows: in Section 2, we recap what is needed of the theory of diffusion processes, their generators, and the conditioning scheme for coarse graining. In Section 3, we prove our main approximation result. We discuss our hypothesis concerning Kramers–Moyal type estimators, as well as its implications for underdamped

Langevin dynamics, in Section 4. Numerical results for two toy problems and two benchmark datasets of molecular dynamics simulation are provided in Section 5. Conclusions and outlook follow in Section 6.

2. Stochastic Dynamics

2.1. Setting

In this paper, we consider a reversible Markov process X_t attaining values in a bounded domain $\Omega \subset \mathbb{R}^d$. The process is governed by the stochastic differential equation

$$dX_t = b(X_t)dt + \sigma(X_t)dB_t. \quad (1)$$

Here, B_t denotes d -dimensional Brownian motion, the function $b : \mathbb{R}^d \mapsto \mathbb{R}^d$ is called the drift, and $\sigma : \mathbb{R}^d \rightarrow \mathbb{R}^{d \times d}$ is called the diffusion. We use the notation $a(x) = \sigma(x)\sigma(x)^T$ for the covariance matrix of the diffusion. A standard example for dynamics of type Eq. (1) are the *overdamped Langevin dynamics*

$$dX_t = -\frac{1}{\gamma}\nabla V(X_t)dt + \sqrt{2\beta^{-1}\gamma^{-1}}dB_t, \quad (2)$$

where $V : \Omega \rightarrow \mathbb{R}$ is a scalar function called the *potential*, while β, γ are constants corresponding to the inverse temperature and the friction in physics applications. We assume that drift and diffusion are smooth functions and that a is bounded and uniformly elliptic, i.e.,

$$\eta_1\|v\|^2 \geq v^T a(x)v \geq \eta_2\|v\|^2, \quad (3)$$

for all vectors $v \in \mathbb{R}^d$, and $\eta_1, \eta_2 > 0$ are independent of x . We assume that X_t is ergodic with respect to a unique invariant measure $d\mu \propto \exp(-F(x))dx$, where F is called a generalized potential. The Hilbert space L_μ^2 consists of all square integrable functions with respect to the measure μ , and the inner product on L_μ^2 is given by

$$\langle \psi, \phi \rangle_\mu = \int_{\mathbb{R}^d} \psi(x)\phi(x) d\mu(x). \quad (4)$$

The *infinitesimal generator* of the Markov process X_t is denoted by \mathcal{L} . For smooth functions with compact support, \mathcal{L} acts as a second order differential operator:

$$\mathcal{L}\psi(x) = b(x) \cdot \nabla\psi(x) + \frac{1}{2}a(x) : \nabla^2\psi(x), \quad (5)$$

where $\nabla^2\psi$ is the Hessian matrix of the function ψ and $:$ denotes the Frobenius inner product between matrices. The generator is symmetric w.r.t. the inner product (4), and it can be extended to a self-adjoint operator on L_μ^2 with domain $\mathcal{D}(\mathcal{L})$, see e.g. [27]. Also, \mathcal{L} satisfies the equality

$$\langle \mathcal{L}\psi, \phi \rangle_\mu = -\frac{1}{2} \int_{\mathbb{R}^d} a(x)\nabla\psi(x) \cdot \nabla\phi(x) d\mu(x). \quad (6)$$

The quadratic form $\mathcal{Q}(\psi, \phi) := -\langle \mathcal{L}\psi, \phi \rangle_\mu$ is defined on either of the Sobolev spaces

$$\mathbb{V}_\mu := H_\mu^{1,0} \quad \text{or} \quad \mathbb{V}_\mu := H_\mu^1, \quad (7)$$

depending on whether \mathcal{L} is equipped with Dirichlet or Neumann boundary conditions. The spectral results in Section 3 will apply in either case.

2.2. Time Evolution and Spectral Decomposition

Given the assumptions outlined above, the generator possesses a complete set of eigenfunctions corresponding to isolated eigenvalues [27, Ch. 6, Thm. 6.3.1], that is, there are functions $1 \equiv \psi_0, \psi_1, \psi_2, \dots$ and non-negative numbers $0 = \kappa_0 < \kappa_1 \leq \dots$ such that

$$-\mathcal{L}\psi_i = \kappa_i\psi_i. \quad (8)$$

The generator gives rise to the semigroup of *Koopman operators* \mathcal{K}_τ , $\tau \geq 0$, defined for $f \in L_\mu^2$ by

$$\mathcal{K}_\tau\psi(x) = \mathbb{E}^x[\psi(X_\tau)],$$

where $\mathbb{E}^x[\cdot]$ denotes expectation given that the dynamics starts deterministically at x , and the time window τ is called the *lag time*. By the spectral mapping theorem [28, Ch 2, Thm 2.4.], the eigenfunctions ψ_i are also eigenfunctions of the Koopman operators \mathcal{K}_τ for all τ , corresponding to eigenvalues

$$\lambda_i(\tau) = e^{-\kappa_i\tau}. \quad (9)$$

Due to the exponential decay of all $\lambda_i(\tau)$, it is common to refer to the κ_i as rates, and to their reciprocals as *implied timescales*

$$t_i = \frac{1}{\kappa_i}. \quad (10)$$

In many applications, including molecular dynamics, we expect to find a number M of dominant rates $0 < \kappa_1 < \dots < \kappa_M \ll \kappa_{M+1}$ separated from all others. The existence of dominant spectral components is directly related to metastability, that is, the existence of long-lived macrostates such that transitions between those states are rare events [29, 30, 31].

2.3. Dimensionality Reduction

We now turn to the dimensionality reduction of a dynamical system onto a smaller number m of variables, and the definition of a suitable effective dynamics. We follow the notation of Refs. [15, 17, 18]. Consider a smooth function ξ which maps the state space $\Omega \subset \mathbb{R}^d$ onto $\hat{\Omega} \subset \mathbb{R}^m$, where $m \leq d$. The *projection operator*

$$\mathcal{P}\psi(z) = \frac{1}{\nu(z)} \int_{\xi^{-1}(z)} \psi(x) \mu(x) J^{-1/2}(x) d\sigma_z(x)$$

computes the stationary average of a function ψ defined on Ω , with σ_z being the surface measure on $\xi^{-1}(z)$ and $J(x)$ the Jacobian determinant of ξ . Moreover, $\nu(z)$ as defined by

$$\nu(z) = \int_{\xi^{-1}(z)} \mu(x) J^{-1/2}(x) d\sigma_z(x) \quad (11)$$

is the ξ -marginal of μ at $\xi(x) = z$. The projection operator is an orthogonal projection onto the subspace [32]

$$\left\{ \psi \in L_\mu^2 : \exists \tilde{\psi} : \hat{\Omega} \rightarrow \mathbb{R}, \psi = \tilde{\psi} \circ \xi \right\},$$

which can be identified with the space L_ν^2 of square-integrable functions on $\hat{\Omega}$ with respect to ν . We do not distinguish between ψ and $\tilde{\psi}$ unless necessary, and we also write $\nabla_z\psi(x)$ for $\nabla_z\tilde{\psi}(\xi(x))$.

As discussed in detail in Ref. [17], an effective dynamics on $\hat{\Omega}$ can be obtained by projection of the generator \mathcal{L} onto the infinite-dimensional space L_ν^2 . Consider the projected generator

$$\mathcal{L}^\xi = \mathcal{P}\mathcal{L}\mathcal{P}, \quad (12)$$

which is a self-adjoint operator on a domain $D(\mathcal{L}^\xi)$. For smooth functions $\psi \in D(\mathcal{L}^\xi)$, it also acts as a differential operator via

$$\mathcal{L}^\xi \psi = \mathcal{P}[\mathcal{L}\xi] \cdot \nabla_z \psi + \frac{1}{2} \mathcal{P}[\nabla \xi^T a \nabla \xi] : \nabla_z^2 \psi, \quad (13)$$

where $\mathcal{L}\xi$ is understood componentwise and $\nabla \xi$ is a $d \times m$ -matrix, $[\nabla \xi]_{il} = \frac{\partial \xi_l}{\partial x_i}$. Thus, \mathcal{L}^ξ is the infinitesimal generator of a reversible diffusion process on $\hat{\Omega}$ with drift and diffusion given by

$$b^\xi(z) = \mathcal{P}(\mathcal{L}\xi)(z), \quad (14)$$

$$a^\xi(z) = \left[\left(\sigma^\xi \right)^T \sigma^\xi \right] (z) = \mathcal{P}(\nabla \xi^T a \nabla \xi)(z). \quad (15)$$

In analogy to Sec. 2.1, the quadratic form for \mathcal{L}^ξ on either of the domains $\mathbb{V}_\nu := H_\nu^{1,0}$ or $\mathbb{V}_\nu := H_\nu^1$ is defined by $\mathcal{Q}^\xi(\cdot, \cdot) = -\langle \mathcal{L}^\xi \cdot, \cdot \rangle_\nu$. An important relation which was also proved in [17] is that, for all $\psi, \phi \in \mathbb{V}_\nu$:

$$\langle \mathcal{L}\psi, \phi \rangle_\mu = -\mathcal{Q}(\psi, \phi) = -\mathcal{Q}^\xi(\psi, \phi) = \left\langle \mathcal{L}^\xi \psi, \phi \right\rangle_\nu. \quad (16)$$

2.4. Galerkin Approximation

The numerical approximation of the eigenfunctions ψ_k , $k = 1, \dots, M$, is often achieved by Galerkin projection. After choosing a finite-dimensional space $\mathbb{W} \subset \mathbb{V}_\mu$, the Galerkin approach consists of finding $\hat{\psi}_i \in \mathbb{W}$ such that

$$Q(\hat{\psi}_i, \phi) = \hat{\omega}_i \langle \hat{\psi}_i, \phi \rangle \quad \forall \phi \in \mathbb{W}. \quad (17)$$

The approximate eigenvalues are also called *Ritz values* associated to \mathbb{W} . From the min-max-principle, we have $\kappa_i \leq \hat{\omega}_i$. If \mathbb{W} is chosen as a subspace of \mathbb{V}_ν (given a set of reduced variables as described in the previous section), it was shown in [17] that (17) serves both as a weak form for \mathcal{L} in \mathbb{V}_μ and for \mathcal{L}^ξ in \mathbb{V}_ν . If we denote the eigenvalues and eigenfunctions of the projected generator $-\mathcal{L}^\xi$ by ϕ_i and ω_i , the min-max principle applied to both \mathcal{L} and \mathcal{L}^ξ shows that

$$\kappa_i \leq \omega_i \leq \hat{\omega}_i \quad (18)$$

for any finite-dimensional subspace $\mathbb{W} \subset \mathbb{V}_\nu$. We will repeatedly use this important insight later on. The Galerkin approach can also be applied to the Koopman operator if $-\mathcal{L}$ is replaced by \mathcal{K}_τ in the definition of the quadratic form. Numerous data-driven approaches to solve the weak eigenvalue problem (17) exist, please refer to [30, 31, 11, 33, 34, 35, 36, 9, 37] and the references therein.

3. Spectral Properties of the Projected Generator

We investigate conditions to ensure that the operator \mathcal{L}^ξ approximately preserves the dominant eigenvalues $\kappa_1, \dots, \kappa_M$, which encode the metastability of the process. To get started, we show that if the derivative of the coarse graining map ξ is full rank everywhere on Ω , including its boundary, the spectrum of \mathcal{L}^ξ is also discrete.

Lemma 3.1. *Let Ω be bounded. Let ξ be continuously differentiable everywhere on $\bar{\Omega}$, and let $\text{rank} \nabla \xi(x) = m$ everywhere on $\bar{\Omega}$. Then the spectrum of \mathcal{L}^ξ is also discrete.*

Proof. The assumptions imply that the smallest eigenvalue of $(\nabla \xi(x))^T \nabla \xi(x)$ is uniformly bounded away from zero by a constant C_λ on $\bar{\Omega}$ and also that $\hat{\Omega}$ is bounded. We conclude that for any unit vector $v \in \mathbb{R}^m$, we have

$$\begin{aligned} v^T a^\xi(z) v &= \frac{1}{\nu(z)} \int_{\xi^{-1}(z)} [v^T (\nabla \xi(x))^T] a(x) [\nabla \xi(x) v] \mu(x) J^{-1/2}(x) d\sigma_z(x) \\ &\geq \frac{\eta_1}{\nu(z)} \int_{\xi^{-1}(z)} \|\nabla \xi(x) v\|^2 \mu(x) J^{-1/2}(x) d\sigma_z(x) \\ &\geq \frac{C_\lambda \eta_1}{\nu(z)} \int_{\xi^{-1}(z)} \mu(x) J^{-1/2}(x) d\sigma_z(x) = C_\lambda \eta_1 > 0. \end{aligned}$$

Hence \mathcal{L}^ξ is uniformly elliptic on the bounded domain $\hat{\Omega}$ and therefore possesses compact resolvents and discrete spectrum. \square

We derive a bound on the eigenvalue error of \mathcal{L}^ξ in terms of the H_μ^1 -approximation error of the dominant eigenfunctions of \mathcal{L} . The idea is to apply classical Galerkin error estimates to a sequence of approximation subspaces in \mathbb{V}_ν , and exploit that these provide approximations to the eigenvalues of both \mathcal{L} and \mathcal{L}^ξ . In what follows, all function spaces are restricted to the orthogonal complement of the constant one function without explicitly changing the notation.

We first introduce the energy norms induced by \mathcal{Q} , \mathcal{Q}^ξ on \mathbb{V}_μ and \mathbb{V}_ν by $\|\cdot\|_{\mathcal{Q}} = [\mathcal{Q}(\cdot, \cdot) + \langle \cdot, \cdot \rangle_\mu]^{1/2}$ and $\|\cdot\|_{\mathcal{Q}^\xi} = [\mathcal{Q}^\xi(\cdot, \cdot) + \langle \cdot, \cdot \rangle_\nu]^{1/2}$. Because of (3) and Lemma 3.1, the energy norms are equivalent to the standard norms on \mathbb{V}_μ and \mathbb{V}_ν , respectively. We will use the symbol $\mathcal{P}_{\mathcal{Q}}$ for the \mathcal{Q} -orthogonal projection onto \mathbb{V}_ν . Second, the solution operator $\mathcal{T} : \mathbb{V}_\mu \rightarrow \mathbb{V}_\mu$ associated to \mathcal{L} is defined by

$$\mathcal{Q}(\mathcal{T}\psi, \phi) = \langle \psi, \phi \rangle_\mu \quad \forall \phi \in \mathbb{V}_\mu.$$

By the assumptions made above on \mathcal{L} , the solution operator is compact. Third, we consider a sequence \mathbb{W}^h of finite-dimensional subspaces of \mathbb{V}_ν . We assume that all \mathbb{W}^h contain the projections $\mathcal{P}_{\mathcal{Q}}\psi_j$ for $j = 1 \dots, M$. Note that the \mathbb{W}^h are just auxiliary spaces which are supposed to exhaust the full space in the limit of $h \rightarrow 0$. There is no need to specify them in detail, and h only serves as a formal parameter here. Finally, the \mathcal{Q} -orthogonal projections from \mathbb{V}_μ onto the spaces \mathbb{W}^h are labeled by \mathcal{P}_h , and the corresponding \mathcal{Q}^ξ -orthogonal projections in \mathbb{V}_ν are called \mathcal{P}_h^ξ . We make the usual approximability assumption on the trial spaces \mathbb{W}^h :

$$\lim_{h \rightarrow 0} \|(\mathcal{I} - \mathcal{P}_h^\xi)\phi\|_{\mathcal{Q}^\xi} = 0 \quad \forall \phi \in \mathbb{V}_\nu. \quad (19)$$

With these preparations, we are ready to prove the following approximation result:

Proposition 3.2. Denote the projection error of eigenfunction ψ_i with respect to the energy-norm by $\delta_i = \|\mathcal{P}_Q^\perp \psi_i\|_Q$. The relative error between the i -th eigenvalues of \mathcal{L}^ξ and \mathcal{L} is bounded by

$$\frac{\omega_i - \kappa_i}{\omega_i} \leq \left[1 + \max_{j=1, \dots, i-1} \frac{\omega_j^2 \kappa_i^2}{(\omega_j - \kappa_i)^2} \|(\mathcal{I} - \mathcal{P}_Q)\mathcal{T}\|_Q^2 \right] \delta_i^2. \quad (20)$$

Proof. Using (18), and by applying [38, Theorem 3.2] to the approximation of \mathcal{L} , we find that for any of the approximation spaces \mathbb{W}^h :

$$\begin{aligned} \frac{\omega_i - \kappa_i}{\omega_i} &\leq \frac{\hat{\omega}_i - \kappa_i}{\hat{\omega}_i} \leq \left[1 + \max_{j=1, \dots, i-1} \frac{\hat{\omega}_j^2 \kappa_i^2}{(\hat{\omega}_j - \kappa_i)^2} \|(\mathcal{I} - \mathcal{P}_h)\mathcal{T}\|_Q^2 \right] \|(\mathcal{I} - \mathcal{P}_h)\psi_i\|_Q^2 \\ &= \left[1 + \max_{j=1, \dots, i-1} \frac{\hat{\omega}_j^2 \kappa_i^2}{(\hat{\omega}_j - \kappa_i)^2} \|(\mathcal{I} - \mathcal{P}_h)\mathcal{T}\|_Q^2 \right] \delta_i^2, \end{aligned}$$

where $\hat{\omega}_i$ are the Ritz values associated to \mathbb{W}^h , see Sec. 2.4. The second equality holds because $\mathcal{P}_Q \psi_i \in \mathbb{W}^h$ by assumption. In the limit of $h \rightarrow 0$, we conclude from (19) that $\hat{\omega}_i \rightarrow \omega_i$, which yields the first term in the pre-factor. For the second term, we first observe that $\mathcal{P}^h = \mathcal{P}_h^\xi \mathcal{P}_Q$, since for any $\psi \in \mathbb{V}_\mu$ and $\phi \in \mathbb{W}^h$:

$$\begin{aligned} \langle \psi - \mathcal{P}_h^\xi \mathcal{P}_Q \psi, \phi \rangle_Q &= \langle (\mathcal{P}_Q + \mathcal{P}_Q^\perp) \psi - \mathcal{P}_h^\xi \mathcal{P}_Q \psi, \phi \rangle_Q \\ &= \langle \mathcal{P}_Q \psi - \mathcal{P}_h^\xi \mathcal{P}_Q \psi, \phi \rangle_Q \\ &= \langle \mathcal{P}_Q \psi - \mathcal{P}_h^\xi \mathcal{P}_Q \psi, \phi \rangle_{Q^\xi} = 0. \end{aligned}$$

The third equality is due to (16), while the last equality is due to the definition of \mathcal{P}_h^ξ . Now, using the pointwise convergence (19) of \mathcal{P}_h^ξ to the identity in \mathbb{V}_ν , we conclude for any $\psi \in \mathbb{V}_\mu$:

$$\begin{aligned} \lim_{h \rightarrow 0} \|(\mathcal{I} - \mathcal{P}_h)\psi - \mathcal{P}_Q^\perp \psi\|_Q &= \lim_{h \rightarrow 0} \|(\mathcal{P}_Q - \mathcal{P}_h)\psi\|_Q \\ &= \lim_{h \rightarrow 0} \|(\mathcal{I} - \mathcal{P}_h^\xi)\mathcal{P}_Q \psi\|_{Q^\xi} = 0. \end{aligned}$$

Combing pointwise convergence of $\mathcal{I} - \mathcal{P}_h$ towards \mathcal{P}_Q^\perp in \mathbb{V}_μ , and compactness of the solution operator, we have

$$\lim_{h \rightarrow 0} (\mathcal{I} - \mathcal{P}_h)\mathcal{T} = (\mathcal{I} - \mathcal{P}_Q)\mathcal{T}$$

with respect to the operator norm. This establishes the proposition. \square

Remark 3.3. Due to the equivalence of the norms $\|\cdot\|_Q$ and $\|\cdot\|_{H_\mu^1}$, the bound in Proposition 3.2 also applies to the latter norm. Let \mathcal{P}_1 denote the orthogonal projection onto \mathbb{V}_ν w.r.t. the standard norm on H_μ^1 . Then

$$\|\mathcal{P}_Q^\perp \psi_i\|_Q \leq \|\mathcal{P}_1^\perp \psi_i\|_Q \leq C \|\mathcal{P}_1^\perp \psi_i\|_{H_\mu^1}.$$

In Ref. [18, Theorem 2], it was shown that the *absolute* eigenvalue error of the projected generator is small if $\|\mathcal{L}\mathcal{P}^\perp\psi_i\|_{L_\mu^2}$ and $\|\mathcal{P}^\perp\psi_i\|_{L_\mu^2}$ are small. Proposition 3.2 complements these results in the sense that it bounds the *relative* error of eigenvalues (timescales), which is a more practical error measure for eigenvalues close to zero, i.e., large timescales. Furthermore, the bound (20) is less restrictive than the conditions in [18], as it uses an H_μ^1 norm instead of the H_μ^2 (or equivalent) norm, as done therein. In fact, the bound assumed in [18, Theorem 2] implies our bound up to another multiplicative constant:

Lemma 3.4. *Let us consider the diffusion (1), satisfying (3), on a bounded domain with smooth boundary and reflecting boundary conditions. If $\|\mathcal{L}\mathcal{P}^\perp\psi_i\|_{L_\mu^2} \leq \delta_i$, then there is a $C > 0$ such that the assumptions of Prop. 3.2 are satisfied with*

$$\|\mathcal{P}^\perp\psi_i\|_{H_\mu^1} \leq C\delta_i. \quad (21)$$

Proof. Since the spatial domain is bounded and μ is smooth, it is a weight in Muckenhoupt class, cf. [39, Eq. (1.2)]. The regularity conditions [39, Eqs. (2.2)–(2.4)] are satisfied by assumption. Now, the result follows directly from the weighted Agmon–Douglis–Nirenberg estimate [39, Theorem 2.4] giving $\|u\|_{H_\mu^2} \leq C\|\mathcal{L}u\|_{L_\mu^2}$ for some $C > 0$ independent of u . We have

$$\begin{aligned} \|\mathcal{P}^\perp\psi_i\|_{H_\mu^1} &\leq \|\mathcal{P}^\perp\psi_i\|_{H_\mu^2} \\ &\leq C\|\mathcal{L}\mathcal{P}^\perp\psi_i\|_{L_\mu^2} \\ &\leq C\delta_i. \end{aligned}$$

concluding the proof. □

4. Kramers–Moyal Formulae and Langevin Dynamics

We now turn to the problem of numerically estimating the coefficients b^ξ , a^ξ from data of the full process X_t . A standard estimator is obtained by averaging the finite difference and the quadratic variation of the process over level sets of ξ , and results in the *Kramers–Moyal formulae* [25]:

$$b^\xi(z) = \lim_{s \rightarrow 0} \mathbb{E} \left[\frac{1}{s} (\xi(X_s) - z) \middle| X_0 \sim \mu_z \right], \quad (22)$$

$$a^\xi(z) = \frac{1}{2} \lim_{s \rightarrow 0} \mathbb{E} \left[\frac{1}{s} (\xi(X_s) - z) \otimes (\xi(X_s) - z) \middle| X_0 \sim \mu_z \right]. \quad (23)$$

Here, μ_z is the measure $\frac{1}{\nu(z)}\mu(x)J^{-1/2}(x) d\sigma_z(x)$ restricted to $\xi^{-1}(z)$, see (11). In practice, Eqs. (22–23) need to be applied at finite s , which can only be expected to constitute a good approximation if s is sufficiently small. However, we present numerical examples where, at least for a good selection of reaction coordinates ξ , the dominant spectrum of the generator is also retained if surprisingly large values of s are used in the estimators above. We state this as a

Conjecture 4.1. Let ξ be a good set of reaction coordinates in the sense of Proposition 3.2. Let $b^{\xi,s}$ and $a^{\xi,s}$ denote the effective drift and diffusion estimated by the Kramers–Moyal formulae (22–23) at $0 < s \leq t_M$. Then the dominant eigenvalues ω_k^s of the generator (13), with b^ξ, a^ξ replaced by $b^{\xi,s}, a^{\xi,s}$ are still close to the original eigenvalues κ_k .

This observation is particularly relevant if the process is governed by the Langevin equation in position and momentum space (q, p) , where $q \in \Omega$ is the position of the system and $p \in \mathbb{R}^d$ is its momentum. The equations of motion are

$$dq_t = p_t dt, \quad (24)$$

$$dp_t = -\nabla V(q_t) dt - \gamma p_t dt + \sqrt{2\gamma\beta^{-1}} dB_t, \quad (25)$$

where V, γ, β have the same physical meaning as in (2) above. The invariant density of the Langevin process factors as $\mu(q, p) = \mu_P(p)\mu_Q(q) \propto \exp(-\frac{\beta}{2}p^T p) \exp(-\beta V(q))$. Oftentimes, the momentum coordinates of the Langevin process equilibrate on timescales much faster than the positions, so performing dimensionality reduction by a map $\xi = \xi(q)$ depending only on the positions is of interest (see [40] for an approach to model reduction which includes the momenta). Unfortunately, the effective dynamics (12) are meaningless in this case, see also [41, 42]. To see this, let us write the pre-image of $z = \xi(q, p)$ as $\xi^{-1}(z) = \xi_q^{-1}(z) \times \mathbb{R}^d$, where $\xi_q^{-1}(z)$ contains all q such that $\xi(q) = z$. Then it is directly verified that $\mathcal{L}\xi = p \cdot \nabla_q \xi$ and $\nabla^T \xi(q) a(q, p) \nabla \xi(q) = 0$. With this, we find

$$\begin{aligned} b^\xi(z) &= \frac{1}{\nu(z)} \int_{\xi_q^{-1}(z) \times \mathbb{R}^d} \mathcal{L}\xi(q, p) \mu(q, p) J^{-1/2}(q) d\sigma_z(q) dp \\ &= \frac{1}{\nu(z)} \int_{\xi_q^{-1}(z) \times \mathbb{R}^d} p \cdot \nabla_q \xi(q) \exp(-\beta V(q)) \exp(-\frac{\beta}{2} p^T p) J^{-1/2}(q) d\sigma_z(q) dp \\ &= \frac{1}{\nu(z)} \int_{\xi_q^{-1}(z)} \exp(-\beta V(q)) J^{-1/2}(q) \nabla_q^T \xi(q) \cdot \left[\int_{\mathbb{R}^d} p \exp(-\frac{\beta}{2} p^T p) dp \right] d\sigma_z(q) \\ &= 0, \\ a^\xi(z) &= \frac{1}{\nu(z)} \int_{\xi_q^{-1}(z)} \nabla^T \xi(q) a(q, p) \nabla \xi(q) \mu(q, p) J^{-1/2}(q) d\sigma_z(q) dp = 0. \end{aligned}$$

However, if the friction γ is sufficiently large, the positional component q_t is close in law to a reversible overdamped dynamics (2) if time is appropriately re-scaled. More precisely, upon the time change $(q_t^\epsilon, p_t^\epsilon) = (q_{t/\epsilon}, p_{t/\epsilon})$, and choosing $\epsilon = \frac{1}{\gamma}$, Eqs. (24–25) transform to

$$dq_t^\epsilon = \frac{1}{\epsilon} p_t^\epsilon dt, \quad (26)$$

$$dp_t^\epsilon = -\frac{1}{\epsilon} \nabla V(q_t^\epsilon) dt - \frac{1}{\epsilon^2} p_t^\epsilon dt + \frac{1}{\epsilon} \sqrt{2\beta^{-1}} dB_t. \quad (27)$$

It follows from the theory of multiscale asymptotics, e.g. [6, Chapter 11], that, as $\epsilon \rightarrow 0$, the re-scaled positional dynamics Eq. (26) converge in law to the overdamped Langevin process

$$dQ_t = -\nabla V(Q_t) dt + \sqrt{2\beta^{-1}} dB_t. \quad (28)$$

Corollary 4.2. *Let ξ be a good reaction coordinate for the overdamped Langevin process $X_t \in \Omega \subset \mathbb{R}^d$ given by (2), in the sense of Prop. 3.2. Let (q_t, p_t) denote the Langevin process on $\Omega \times \mathbb{R}^d$.*

(i) *For γ sufficiently large, the statistics of the positional component q_t of the Langevin process, and of the overdamped process X_t , approximately agree on timescales much larger than $\frac{1}{\gamma}$.*

(ii) *If in addition Conjecture 4.1 is true, then application of the Kramers–Moyal formulae at $t_M > s > \frac{1}{\gamma}$ to q_t results in an effective dynamics on $\xi(\Omega)$ which approximately retains the dominant timescales of X_t .*

Proof. (i) If we re-scale the Langevin process (24 - 25) by $(q_t^c, p_t^c) = (q_{c\gamma t}, p_{c\gamma t}) = (q_{ct/\epsilon}, p_{ct/\epsilon})$, the re-scaled equations of motion are

$$\begin{aligned} dq_t^c &= \frac{c}{\epsilon} p_t^c dt, \\ dp_t^c &= -\frac{c}{\epsilon} \nabla V(q_t^c) dt - \frac{c}{\epsilon^2} p_t^c dt + \frac{1}{\epsilon} \sqrt{2\beta^{-1}c} dB_t. \end{aligned}$$

For sufficiently large γ and $c \geq 1$, Theorem 18.1 of [6] implies that the law of q_t^c is close to that of

$$dQ_t^c = -c \nabla V(Q_t^c) dt + \sqrt{2\beta^{-1}c} dB_t.$$

We note that Q_t^c is a time re-scaling of X_t via $Q_t^c = X_{c\gamma t}$, hence we have for suitable functions $f = f(q)$:

$$\mathbb{E}^{\mu_Q} [f(q_{c\gamma t})] \approx \mathbb{E}^{\mu_Q} [f(X_{c\gamma t})]. \quad (29)$$

(ii) In particular, the approximate equality (29) applies to the conditional expectations in (22 - 23) for $s > \frac{1}{\gamma}$. If conjecture 4.1 is true, the resulting effective dynamics will retain the leading timescales of the process X_t . \square

5. Numerical Examples

In this section, we use several examples to illustrate the error estimates obtained in Prop. 3.2, and to support the conjecture made in Section 4. To this end, we first project each of the test systems onto a suitable one- or two-dimensional reaction coordinate. The choice of reaction coordinate is either based on knowledge of the system or on numerical approximation of the full generator. We then apply the Kramers–Moyal estimators Eqs. (22 - 23) to approximate the effective drift and diffusion. We do so using a range of different values for the offset parameter s in (22 - 23). For each set of parameters thus obtained, we integrate the resulting low-dimensional dynamics numerically. The resulting data are re-analyzed in order to compare the spectral properties of the low-dimensional dynamics to those of the full dynamical system. Before going into the details of each example, we discuss some of the numerical techniques employed in each case.

Kramers–Moyal Estimators Since all of the examples below are rather simple systems, we have long equilibrium simulations of the full process X_t at our disposal. We then discretize the reaction coordinate space into evenly spaced bins B_i . For each of these bins, all simulation steps X_t such that $\xi(X_t)$ falls into B_i are determined. As the data are in global

equilibrium, we can then average the linear and quadratic differences $\frac{1}{s}(\xi(X_{t+s}) - \xi(X_t))$ and $\frac{1}{s}(\xi(X_{t+s}) - \xi(X_t)) \otimes (\xi(X_{t+s}) - \xi(X_t))$ over all $X_t \in S_i$ to obtain discretized estimates of effective drift and diffusion. These estimates are extended to continuous space by interpolation. We are aware that this procedure is only feasible for low-dimensional reaction coordinate spaces and if the simulation of an equilibrium trajectory is possible. There is a huge body of literature on estimating equilibrium expectations from non-equilibrium data (e.g. [43, 44, 45]) and on obtaining functional representations of the drift and diffusion from data ([23, 26]), but these problems are beyond the scope of this study.

Simulation of the Effective Dynamics After interpolating the discretized estimates of the effective drift and diffusion, we can evaluate the parameters of the effective dynamics at any point in reaction coordinate space. Therefore, we can simply apply the standard Euler-Maruyama integrator to obtain an equilibrium trajectory of the coarse-grained system. The integration time step and total simulation time of these realizations are chosen to be the same as those of the original time series for X_t .

Markov State Models Simulation data of the effective dynamics are analyzed by Markov State Models (MSMs), which provide a Galerkin approximation of the Koopman operator \mathcal{K}_τ based on indicator functions corresponding to a box partitioning of state space. The same discrete bins as for the application of the Kramers–Moyal formulae are used to define the partitioning. The pyemma software package [46] is used to estimate MSMs from data, and standard protocols [11, 35] are employed to select a suitable lag time τ . Leading eigenvalues of the MSM serve as approximations to the true eigenvalues of the Koopman operator \mathcal{K}_τ . As these eigenvalues are functions of the lag time, we use (9) and (10) to convert them into implied timescales, which can be compared to those of the original generator \mathcal{L} . The PCCA algorithm [47, 48] can be applied to the dominant eigenvectors of the MSM, in order to obtain a decomposition of state space into a few metastable sets. As the first left eigenvector of an MSM provides an estimate of the equilibrium probabilities of all discrete states, we can also calculate stationary probabilities of the metastable states, serving as another comparison to the original dynamical system.

5.1. Lemon Slice Potential

The first example serves to illustrate the validity of Proposition 3.2 and to demonstrate that using a large offset s in the Kramers–Moyal formulae does not impair the quality of approximation for essential stationary and dynamical quantities. We consider overdamped Langevin dynamics Eq. (2) in the lemon slice potential

$$V(r, \varphi) = \cos(7\varphi) + 10(r - 1)^2 + \frac{1}{r} + 0.05, \quad (30)$$

where r, φ are two-dimensional polar coordinates, at inverse temperature $\beta = 1$ and friction $\gamma = 1$. It is known from previous studies [32] that transitions between the seven minima shown in Fig. 1 constitute the slow dynamics of this system. Hence, we select the polar angle φ as reaction coordinate $\xi(x, y) = \varphi(x, y)$. In this case, the effective drift b^ξ and diffusion a^ξ can be calculated analytically, see appendix A. We generate a long equilibrium simulation of the dynamics Eq. (2) using the Euler–Maruyama method at integration time

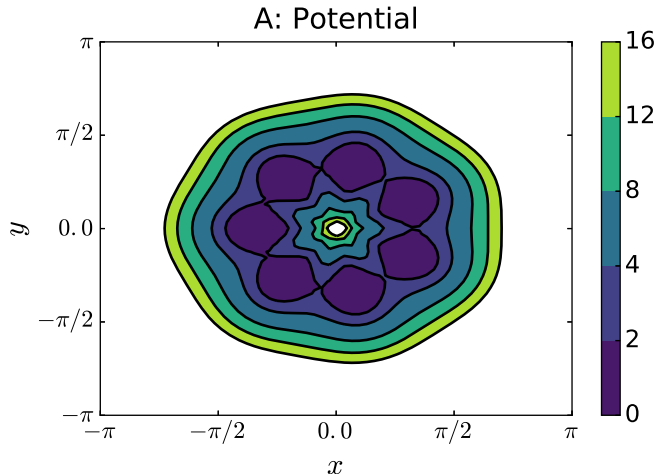


Figure 1: Contour plot of the lemon slice potential Eq. (30).

step $\Delta_t = 10^{-3}$ for a total of 10^7 steps. A Markov state model analysis—as described above—of the full data set reveals seven dominant eigenvalues and six corresponding slow timescales t_1, \dots, t_6 . These slow timescales come in three pairs due to the symmetry of the system.

Parameters of the effective dynamics are estimated using 63 discrete bins along the angular coordinate. Offsets s range between the integration time step $s = 10^{-3}$ and $s = 1.0$. We can observe in Figs. 2 A and B that the exact drift and diffusion are recovered well for small s , while very different results are obtained as s increases. In particular, the effective diffusion is no longer constant as a function of ξ for large s . Nevertheless, as shown in Fig. 2 C, estimates of the six leading implied timescales based on the effective dynamics barely change as s increases. This is expected for small s due to Proposition 3.2, but it is unexpected for large s . We also monitor the stationary probabilities of the seven potential minima if estimated from different effective simulations. The minima are defined as intervals $z \in [z_k - 0.25, z_k + 0.25]$ for $z_k = -\pi + \frac{2\pi k}{7}$, $k = 0, \dots, 6$. We compare them to the reference obtained by numerically integrating the marginal $\nu(z)$, Eq. (11), over those intervals. In Fig. 2 D, we find that these probabilities are preserved by the effective dynamics until s is comparable to $t_5 = t_6$. Thus, the essential stationary and dynamical properties of the original dynamics seem to be preserved even if the effective dynamics are estimated at fairly large offset s .

5.2. Langevin Toy Model

The purpose of the next example is to illustrate that using a large offset s is actually necessary to define reliable effective dynamics if Langevin dynamics are projected onto a reaction coordinate ξ which is independent of the momenta. We study another two-dimensional toy potential composed of a double-well in x -direction and harmonic potentials in both x and y , the functional form is

$$V(x, y) = 1.5(x - 2)^4 - 9(x - 2)^2 + 3x + 0.5(x - 2)^2 + 0.5(y - 2)^2. \quad (31)$$

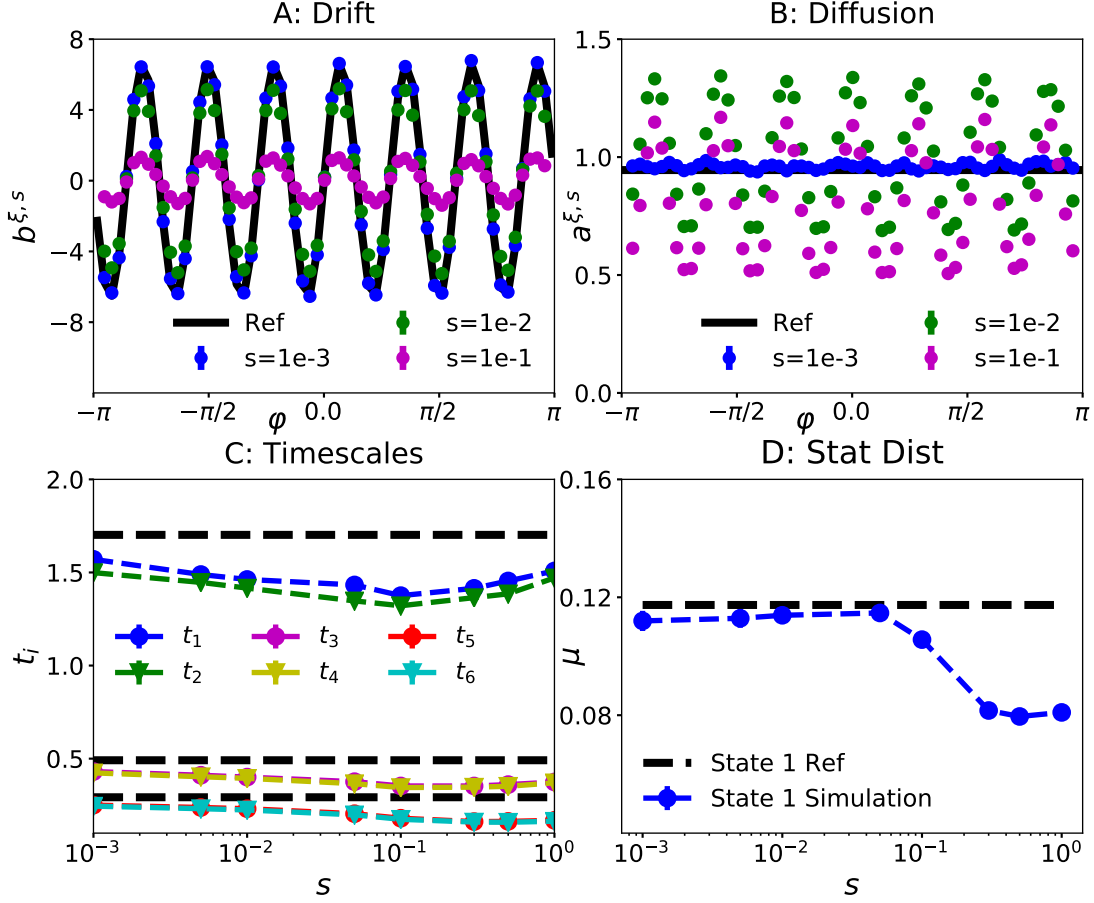


Figure 2: Analysis of effective dynamics on the polar angle for the lemon slice potential. A: Numerical estimates of effective drift for different values of the offset s , compared to the reference in black. B: The same for the effective diffusion. C: Implied timescales t_1, \dots, t_6 obtained by analyzing simulation data of the effective dynamics, as a function of s , compared to the reference values in black. Note that all of these timescales come in three pairs due to the symmetry of the system. D: Stationary probabilities of one of the potential minima estimated from simulations of the effective dynamics, as a function of s . The reference value is shown in black. Errorbars were produced by bootstrapping on the original data (A and B) and on the effective simulations (C and D). We note that errorbars in C and D are barely visible.

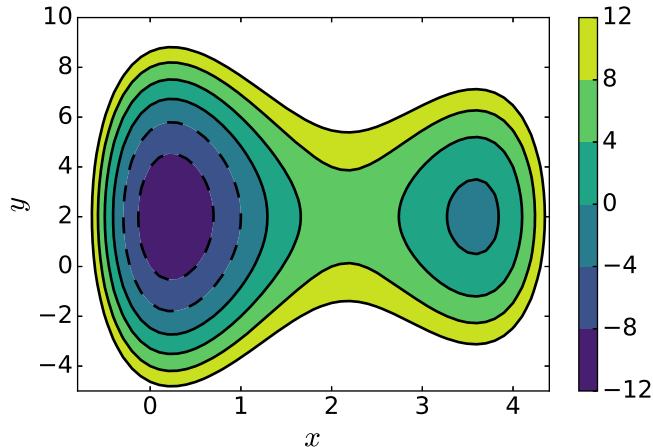


Figure 3: Contour plot of the two-dimensional toy potential Eq. (31).

A contour plot of V is shown in Fig. 3. For both Langevin and overdamped Langevin dynamics, the slowest transition in this energy landscape is the crossing of the barrier around $x = 2$, thus $\xi = x$ is a good reaction coordinate in the sense of Proposition 3.2.

We simulate Langevin dynamics ($\gamma = 10$, $\beta = 0.4$) using the Euler–Maruyama scheme at integration time step $\Delta_t = 10^{-2}$ for 10^7 steps, and also generate data of the overdamped dynamics in the same potential using the same simulation parameters. Figures 4 A and B show numerical estimates of the effective drift and diffusion obtained by the Kramers–Moyal formulae along 24 discrete bins, using both the Langevin and overdamped Langevin simulations. We note that these estimates are very different for $s = 0.01$ (and in agreement with Section 4, estimates from Langevin data are close to zero), but they agree for $s = 1.0$. We extract the slowest implied timescale t_1 and the probabilities of two metastable sets from all effective simulations. For sufficiently large s , all effective simulations reproduce both t_1 (Fig. 4 C) and the probabilities of the PCCA sets (Fig. 4 D) from the original simulations of the overdamped dynamics.

This example shows that upon increasing the offset it is possible to find a sweet spot where s is larger than the momentum relaxation time $\frac{1}{\gamma}$, but smaller than the slowest timescale t_1 such that meaningful effective dynamics along x can be defined in this regime.

5.3. Alanine Dipeptide

We move on to a more complex example, which is a dataset of molecular dynamics simulations of alanine dipeptide. This small molecule has been used as a test system for method development many times in recent years. Its slow dynamics can be represented in the space of backbone dihedral angles ϕ , ψ . We only focus on the slowest process, which is the crossing of the highest free energy barrier at $\phi = 0$ along the direction of the ϕ -angle, see Figure 5 A. Therefore we choose $\xi(x) = \phi(x)$ as one-dimensional reaction coordinate in this example.

The data consists of 20 long simulations of 200 ns simulation time each. The detailed simulation setup can be found on Ref. [49]. The dynamical model for these simulations is the velocity re-scaling thermostat, with time constant $\tau_v = 0.01$ ps. Velocity re-scaling is

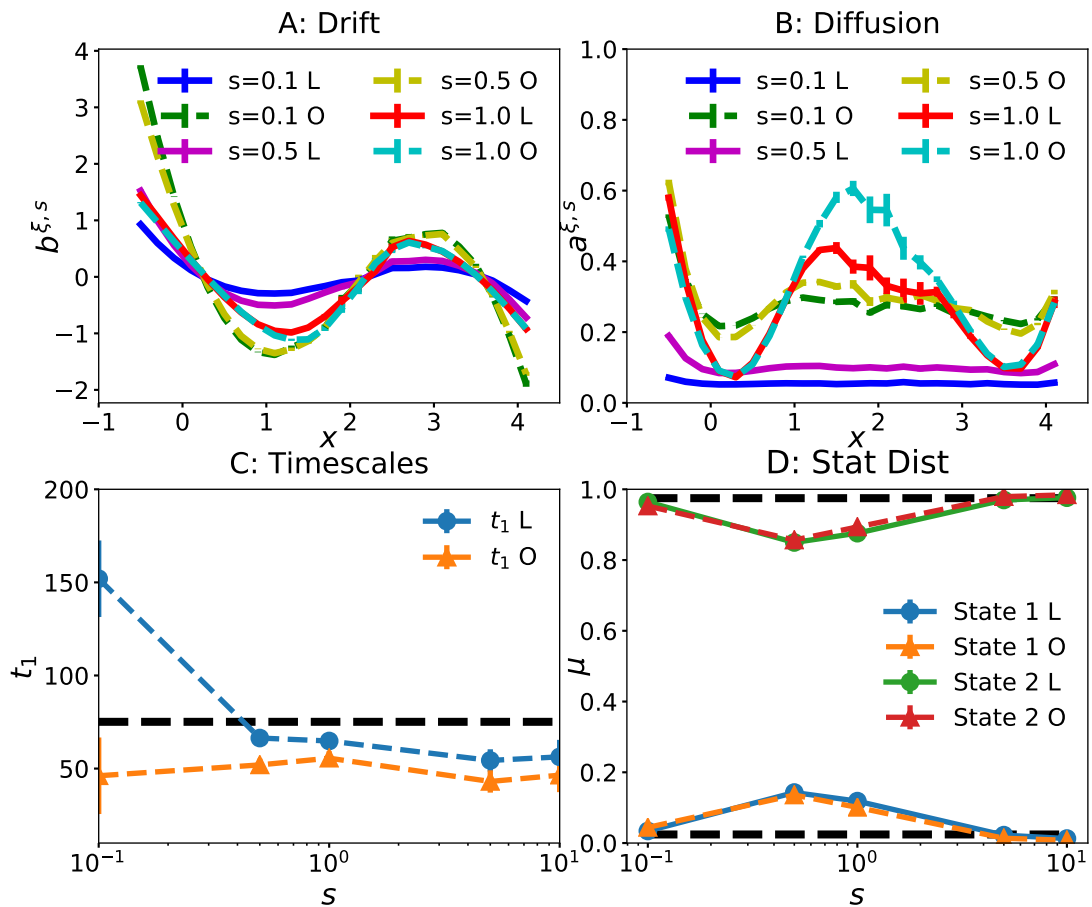


Figure 4: Analysis of effective dynamics on the x -coordinate of the two-dimensional toy potential Eq. (31). A: Numerical estimates of effective drift for different values of the offset s using both the Langevin data (L) and the overdamped data (O). B: The same for the effective diffusion. C: Leading implied timescale t_1 obtained by analyzing simulation data of the effective dynamics from both Langevin data (blue) and overdamped data (orange), as a function of s , compared to the reference value in black. D: Stationary probabilities of the two metastable sets estimated from simulations of the effective dynamics from both Langevin data (circles) and overdamped data (triangles), as a function of s , compared to the references in black. Errorbars were produced by bootstrapping on the original data (A and B) and on the effective simulations (C and D). We note that errorbars in C and D are barely visible.

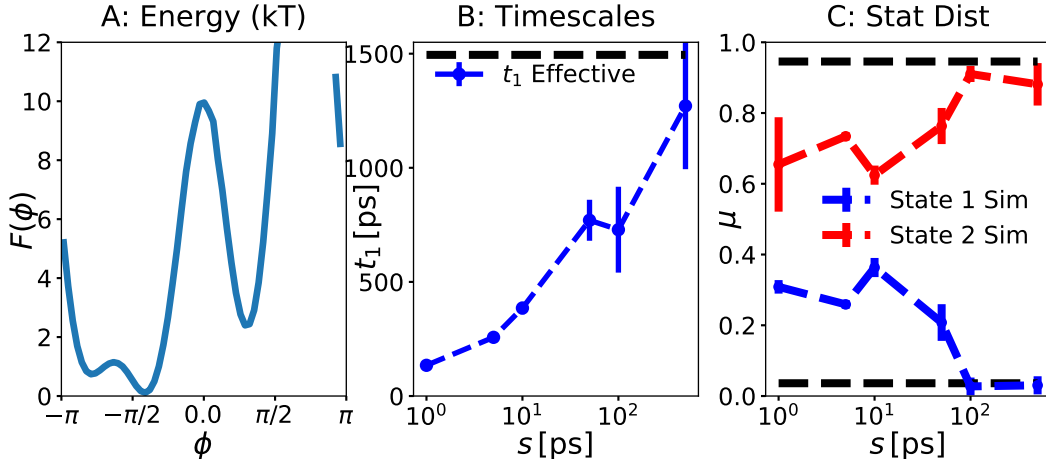


Figure 5: Analysis of effective dynamics for alanine dipeptide along ϕ -direction. A: Effective free energy of the original simulation data as a function of ϕ . B: Slowest implied timescale t_1 obtained from a Markov state model of the effective dynamics, as a function of s . The reference value is indicated by the black line. C: Stationary probabilities of two PCCA sets extracted from the effective dynamics, as a function of s . Black lines indicate stationary probabilities of metastable sets extracted from the original data. Errorbars in panels C and D were obtained by bootstrapping on the effective simulations.

closely related to Langevin dynamics, with τ_v playing the role of friction γ [50]. A Markov state model based on 500 discrete bins in ϕ - ψ -space serves as reference model for timescales and equilibrium probabilities.

The effective drift and diffusion are estimated for 62 discrete bins along the ϕ -coordinate. Offsets range from $s = 1$ ps up to $s = 500$ ps. Panel B of Figure 5 shows the slowest implied timescale estimated by Markov state models of these effective simulations, as a function of the offset s . It can be observed that the slowest timescale is clearly underestimated at small s , but estimates improve with increasing s and the correct regime is reached for $s \geq 100$ ps $= \frac{1}{\tau_v}$. The same observation can be made for equilibrium probabilities of the two metastable sets extracted from the Markov models, see Fig. 5 C. We are thus able to confirm the findings of the previous section for a more complex dynamical system.

5.4. Deca Alanine

We conclude by studying another molecular example, namely simulations of the deca alanine peptide. We use a data set of six independent long simulations of 500 ns each, with velocity re-scaling time constant $\tau_v = 0.01$ ps. Again, please refer to Ref. [49] for the detailed simulation setup.

This time, we cannot choose the reaction coordinates based on knowledge or intuition, so we select a projection into the space of two slowest approximate eigenfunctions, that is $\xi(x) = [\hat{\psi}_1(x), \hat{\psi}_2(x)] \in \mathbb{R}^2$, where $\hat{\psi}_1 \approx \psi_1$, $\hat{\psi}_2 \approx \psi_2$. These approximations are obtained by following a standard procedure to obtain a Galerkin approximation of the Koopman operator; the details are provided in Appendix B. The upper part of Fig. 6 A shows the

free energy $-\log(\nu(z))$ in the reaction coordinate space, where three major minima can be identified.

We use 784 bins of size 0.1×0.1 in the projected space to estimate effective drift and diffusion for a series of offsets between $s = 1$ ps and $s = 1$ ns. We extract the two leading implied timescales from the simulations of all these models, and compare them to those of the original simulation in Fig. 6 B. Our findings are similar to what we observed for the alanine dipeptide. Both timescales are massively underestimated at small s , but agree much better as s increases past $\frac{1}{\tau_v} = 100$ ps. In Fig. 6 A, lower part, we show the effective free energy sampled by the simulation at $s = 1$ ns. It can be seen that detailed features of the original energy landscape are washed out, only the overall structure of valleys and barriers is roughly preserved. Nevertheless, comparing the stationary probabilities of the three PCCA sets obtained from the original dynamics in both the original and effective simulations, we find that these probabilities are approximately preserved for $s = 1$ ns. In fact, they are preserved for most values of s in this example, see Fig. 6 C.

6. Conclusions

We have discussed the approximation of high-dimensional diffusion processes by effective dynamics defined on the lower-dimensional space of reduced variables. We have analyzed the approximation quality of low-lying eigenvalues of the corresponding generator for reversible diffusions. A new relative error bound for dominant eigenvalues in terms of the H_μ^1 -approximation error of the corresponding eigenfunctions was proved. Furthermore, we have discussed how the overdamped limit can be exploited to extend the validity of these approximation results to Langevin dynamics. Numerical examples have shown that using a large offset in the Kramers–Moyal estimators for effective drift and diffusion coefficients does not seem to impair the approximation quality of dominant eigenvalues. Future work will focus on providing a theoretical foundation for the observations stated in Conjecture 4.1. Also, the relation between the positional coordinate of an (underdamped) Langevin process on long timescales, and the corresponding overdamped Langevin equation (cf. Corollary 4.2 (i)), needs to be analyzed in more detail.

Funding and Acknowledgments

This research was funded by Rice University Academy of Fellows (F.N.), by Deutsche Forschungsgemeinschaft (DFG) through CRC 1114 "Scaling Cascades in Complex Systems", project A01 (P.K.), by the Einstein Foundation Berlin (C.C.), by the National Science Foundation (Nos. CHE-1265929, CHE- 1738990, and PHY-1427654) and the Welch Foundation (No. C-1570) (F.N., L.B., C.C.).

We would like to thank Ralf Banisch, Stefan Klus, Thomas Swinburne, Tony Lelièvre and Frank Noé. We are also indebted to the Institute for Pure and Applied Mathematics (IPAM) for hosting the long program "Complex High-Dimensional Energy Landscapes".

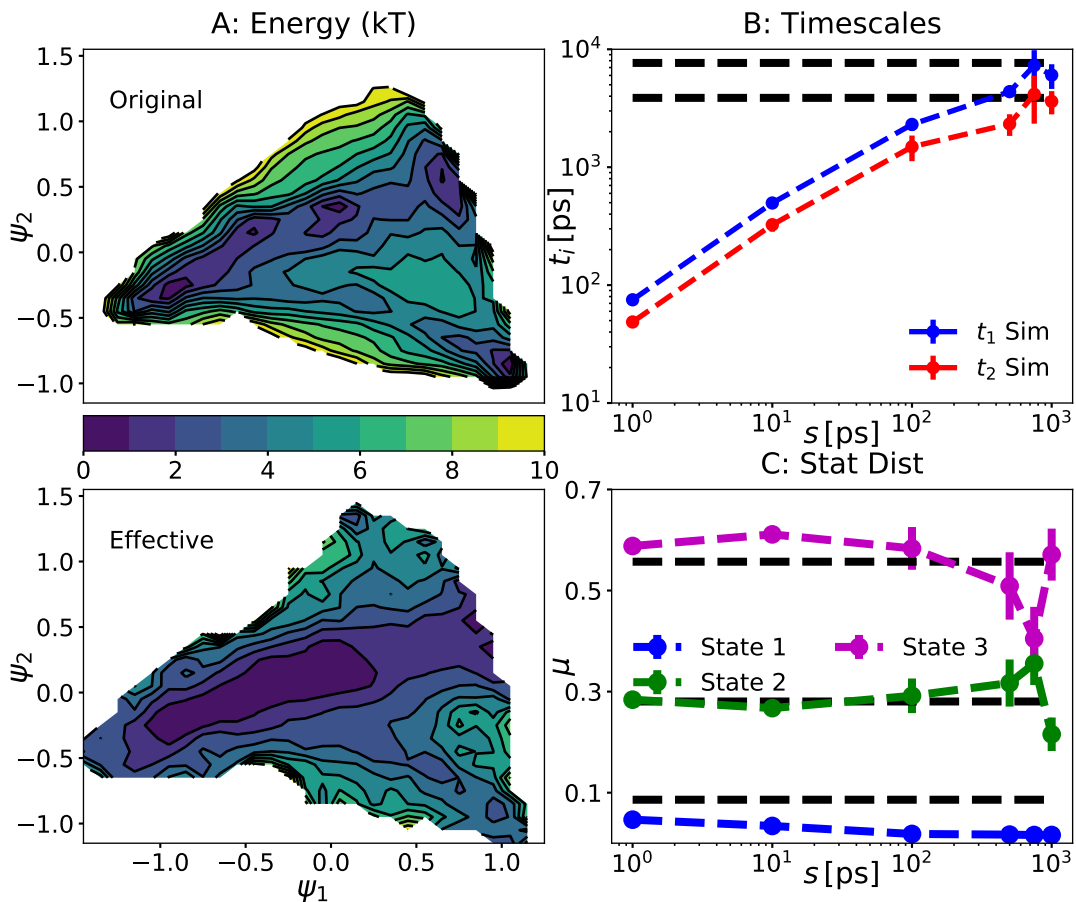


Figure 6: Analysis of effective dynamics for deca alanine in the space of its two slowest eigenfunctions. A: Effective free energy of the original dynamics (top) and free energy sampled by effective dynamics at $s = 1$ ns (bottom). B: First two implied timescales of the effective simulations as a function of the offset s , compared to the references in black. C: Stationary probabilities of three metastable sets (obtained from the original data using the PCCA method) as a function of s , compared to the reference values (black lines). Errorbars in panels B and C were obtained by bootstrapping on the effective simulations.

References

- [1] H. Mori. Transport, collective motion, and Brownian motion. *Prog. Theor. Phys.*, 33:423–455, 1965.
- [2] R. Zwanzig. Nonlinear generalized Langevin equations. *J. Stat. Phys.*, 9(3):215–220, 1973.
- [3] A. J. Chorin, O. H. Hald, and R. Kupferman. Optimal prediction and the Mori–Zwanzig representation of irreversible processes. *Proc. Natl. Acad. Sci. U.S.A.*, 97(7):2968–2973, 2000.
- [4] A. J. Chorin, O. H. Hald, and R. Kupferman. Optimal prediction with memory. *Physica D*, 166(3):239–257, 2002.
- [5] C. Hijón, P. Español, E. Vanden-Eijnden, and R. Delgado-Buscalioni. Mori–Zwanzig formalism as a practical computational tool. *Faraday Discuss.*, 144(0):301–322, 2009.

- [6] G. Pavliotis and A. Stuart. *Multiscale methods: averaging and homogenization*. Springer Science & Business Media, 2008.
- [7] G. A. Pavliotis and A. M. Stuart. Parameter estimation for multiscale diffusions. *J. Stat. Phys.*, 127(4):741–781, 2007.
- [8] C. Clementi. Coarse-grained models of protein folding: Tol-models or predictive tools? *Curr. Opin. Struct. Biol.*, 18:10–15, 2008.
- [9] F. Noé and C. Clementi. Collective variables for the study of long-time kinetics from molecular trajectories: theory and methods. *Curr. Opin. Struct. Biol.*, 43:141–147, 2017.
- [10] W.G. Noid. Perspective: Coarse-grained models for biomolecular systems. *J. Phys. Chem.*, 139(9):090901, 2013.
- [11] J.-H. Prinz, H Wu, M Sarich, B Keller, M Senne, M Held, J D Chodera, C Schütte, and F Noé. Markov models of molecular kinetics: Generation and Validation. *J. Chem. Phys.*, 134:174105, 2011.
- [12] M. A. Rohrdanz, W. Zheng, M. Maggioni, and C. Clementi. Determination of reaction coordinates via locally scaled diffusion map. *J. Chem. Phys.*, 134:124116, 2011.
- [13] M. G. Saunders and G. A. Voth. Coarse-graining methods for computational biology. *Annu. Rev. Biophys.*, 42(1):73–93, 2013.
- [14] W. E and E. Vanden-Eijnden. Metastability, conformation dynamics, and transition pathways in complex systems. In *Multiscale modelling and simulation*, pages 35–68. Springer, 2004.
- [15] F. Legoll and T. Lelièvre. Effective dynamics using conditional expectations. *Nonlinearity*, 23(9):2131, 2010.
- [16] G. Froyland, G. A. Gottwald, and A. Hammerlindl. A trajectory-free framework for analysing multiscale systems. *Physica D*, 328:34–43, 2016.
- [17] W. Zhang, C. Hartmann, and C. Schutte. Effective dynamics along given reaction coordinates, and reaction rate theory. *Faraday Discuss.*, 195:365–394, 2016.
- [18] W. Zhang and C. Schütte. Reliable Approximation of Long Relaxation Timescales in Molecular Dynamics. *Entropy*, 19(7), 2017.
- [19] F. Legoll, T. Lelièvre, and S. Olla. Pathwise estimates for an effective dynamics. *Stochastic Processes Appl.*, 127(9):2841–2863, 2017.
- [20] T. Lelièvre and W. Zhang. Pathwise estimates for effective dynamics: the case of nonlinear vectorial reaction coordinates. *Multiscale Model. Simul.*, 17(3):1019–1051, 2019.
- [21] M. Kessler, A. Lindner, and M. Sorensen. *Statistical methods for stochastic differential equations*. CRC Press, 2012.
- [22] E. Gobet, M. Hoffmann, and M. Reiß. Nonparametric estimation of scalar diffusions based on low frequency data. *Ann. Stat.*, 32(5):2223–2253, 2004.
- [23] D. Crommelin and E. Vanden-Eijnden. Diffusion Estimation from Multiscale Data by Operator Eigenpairs. *Multiscale Model. Simul.*, 9(4):1588–1623, 2011.
- [24] L. Zhang, P. A. Mykland, and Y. Aït-Sahalia. A tale of two time scales: Determining integrated volatility with noisy high-frequency data. *J. Am. Stat. Assoc.*, 100(472):1394–1411, 2005.
- [25] H. Risken and H. Haken. *The Fokker-Planck Equation: Methods of Solution and Applications Second Edition*. Springer, 1989.

- [26] L. Boninsegna, F. Nüske, and C. Clementi. Sparse learning of stochastic dynamical equations. *J. Chem. Phys.*, 148(24):241723, 2018.
- [27] E. B. Davies. *Spectral theory and differential operators*, volume 42. Cambridge University Press, 1996.
- [28] A. Pazy. *Semigroups of linear operators and applications to partial differential equations*. Springer, New York, Berlin, 1983.
- [29] E. B. Davies. Metastable states of symmetric Markov semigroups I. *Proc. London Math. Soc.*, 45:133–150, 1982.
- [30] M. Dellnitz and O. Junge. On the Approximation of Complicated Dynamical Behavior. *SIAM J. Numer. Anal.*, 36(2):491–515, 1999.
- [31] P. Deuffhard, W. Huisinga, A. Fischer, and C. Schütte. Identification of almost invariant aggregates in reversible nearly uncoupled Markov chains. *Linear Algebra Appl.*, 315(1-3):39–59, 2000.
- [32] A. Bittracher, P. Koltai, S. Klus, R. Banisch, M. Dellnitz, and C. Schütte. Transition Manifolds of Complex Metastable Systems: Theory and Data-Driven Computation of Effective Dynamics. *J. Nonlinear Sci.*, (Md):1–42, 2017.
- [33] C. Schütte and M. Sarich. *Metastability and Markov State Models in Molecular Dynamics: Modeling, Analysis, Algorithmic Approaches*. Courant Lecture Notes. American Mathematical Society and Courant Institute of Mathematical Sciences, 2013.
- [34] F. Noé and F. Nüske. A variational approach to modeling slow processes in stochastic dynamical systems. *Multiscale Model. Simul.*, 11:635–655, 2013.
- [35] G. R. Bowman, V. S. Pande, and F. Noé, editors. *An Introduction to Markov State Models and Their Application to Long Timescale Molecular Simulation*. Springer Netherlands, 2014.
- [36] M. O. Williams, I. G. Kevrekidis, and C. W. Rowley. A data-driven approximation of the Koopman operator: Extending dynamic mode decomposition. *J. Nonlinear Sci.*, 25(6):1307–1346, 2015. doi:10.1007/s00332-015-9258-5.
- [37] S. Klus, F. Nüske, P. Koltai, H. Wu, I. Kevrekidis, C. Schütte, and F. Noé. Data-Driven Model Reduction and Transfer Operator Approximation. *J. Nonlinear Sci.*, 2018.
- [38] A. V. Knyazev and J. E. Osborn. New a priori fem error estimates for eigenvalues. *SIAM J. Numer. Anal.*, 43(6):2647–2667, 2006.
- [39] M. E. Cejas and R. G. Durán. Weighted a priori estimates for elliptic equations. *Studia Mathematica*, 2018.
- [40] M. H. Duong, A. Lamacz, M. A. Peletier, A. Schlichting, and U. Sharma. Quantification of coarse-graining error in langevin and overdamped langevin dynamics. *Nonlinearity*, 31(10):4517, 2018.
- [41] C. Schütte. *Conformational dynamics: Modelling, theory, algorithm, and application to biomolecules*. 1999.
- [42] A. Bittracher, P. Koltai, and O. Junge. Pseudogenerators of spatial transfer operators. *SIAM J. Appl. Dyn. Syst.*, 14(3):1478–1517, 2015.
- [43] H. Wu, F. Nüske, F. Paul, S. Klus, P. Koltai, and F. Noé. Variational approximation of molecular kinetics from short off-equilibrium simulations. *J. Chem. Phys.*, 2017.
- [44] F. Nüske, H. Wu, J.-H. Prinz, C. Wehmeyer, C. Clementi, and F. Noé. Markov state models from short non-equilibrium simulations — Analysis and correction of estimation bias. *J. Chem. Phys.*, 094104, 2017.

- [45] P. Koltai, H. Wu, F. Noé, and C. Schütte. Optimal data-driven estimation of generalized Markov state models for non-equilibrium dynamics. *Computation*, 6(1):22, 2018.
- [46] M. K. Scherer, B. Trendelkamp-Schroer, F. Paul, G. Pérez-Hernández, M. Hoffmann, N. Plattner, C. Wehmeyer, J.-H. Prinz, and F. Noé. Pyemma 2: A software package for estimation, validation, and analysis of markov models. *J. Chem. Theory Comput.*, 11(11):5525–5542, 2015.
- [47] P. Deuffhard and M. Weber. Robust Perron cluster analysis in conformation dynamics. *Linear Algebra Appl.*, 398:161–184, 2005.
- [48] S. Röblitz and M. Weber. Fuzzy spectral clustering by PCCA+: Application to Markov state models and data classification. *Adv. Data Anal. Classif.*, 7(2):147–179, 2013.
- [49] F. Nüske, B. G. Keller, G. Pérez-Hernández, A. S. J. S. Mey, and F. Noé. Variational Approach to Molecular Kinetics. *J. Chem. Theory Comput.*, 10:1739–1752, 2014.
- [50] G. Bussi and M. Parrinello. Stochastic thermostats: comparison of local and global schemes. *Comput. Phys. Commun.*, 179(1-3):26–29, 2008.
- [51] G. Pérez-Hernández, F. Paul, T. Giorgino, G. De Fabritiis, and F. Noé. Identification of slow molecular order parameters for Markov model construction. *J. Chem. Phys.*, 139(1):15102, 2013.
- [52] F. Noé and C. Clementi. Kinetic Distance and Kinetic Maps from Molecular Dynamics Simulation. *J. Chem. Theory Comput.*, 11(10):5002–5011, 2015.

A. Lemon Slice Potential

Here, we calculate the effective drift and diffusion if the lemon slice potential Eq. (30) is projected onto the polar angle $\xi(x, y) = \varphi(x, y)$. We start by expressing the generator \mathcal{L} in polar coordinates. The Laplacian operator in polar coordinates is

$$\Delta f = \frac{\partial^2 f}{\partial r^2} + \frac{1}{r^2} \frac{\partial^2 f}{\partial \varphi^2} + \frac{1}{r} \frac{\partial f}{\partial r}.$$

Moreover, it follows from the chain rule and the definition of ξ that for any function f ,

$$\begin{aligned} \frac{\partial f}{\partial x} &= \cos \varphi \frac{\partial f}{\partial r} - \frac{\sin \varphi}{r} \frac{\partial f}{\partial \varphi}, \\ \frac{\partial f}{\partial y} &= \sin \varphi \frac{\partial f}{\partial r} + \frac{\cos \varphi}{r} \frac{\partial f}{\partial \varphi}. \end{aligned}$$

The generator in polar coordinates then becomes

$$\mathcal{L} = - \left[\frac{\partial V}{\partial r} \frac{\partial}{\partial r} + \frac{1}{r^2} \frac{\partial V}{\partial \varphi} \frac{\partial}{\partial \varphi} \right] + \frac{1}{\beta} \left[\frac{\partial^2}{\partial r^2} + \frac{1}{r^2} \frac{\partial^2}{\partial \varphi^2} + \frac{1}{r} \frac{\partial}{\partial r} \right].$$

Applying the generator to the reaction coordinate ξ , only one of the terms above is non-zero, resulting in

$$\mathcal{L}\xi = -\frac{1}{r^2} \frac{\partial V}{\partial \varphi} = \frac{7}{r^2} \sin(7\varphi)$$

In order to evaluate Eq. (14), we note that the Jacobian determinant of ξ is $J(x, y) = \frac{1}{r^2}$, and that the stationary distribution factors, canceling the φ -dependent and the constant term. We are left with

$$\begin{aligned} b^\xi(\varphi) &= \frac{1}{\nu(\varphi)} \int_0^\infty \frac{7}{r^2} \sin(7\varphi) r \mu(r, \varphi) dr \\ &= \frac{7}{C_2} \sin(7\varphi) \int_0^\infty \frac{1}{r} \exp(-10(r-1)^2 - \frac{1}{r}) dr \\ &= \frac{7C_1}{C_2} \sin(7\varphi), \end{aligned}$$

with the definitions $C_1 := \int_0^\infty \frac{1}{r} \exp(-10(r-1)^2 - \frac{1}{r}) dr$ and $C_2 := \int_0^\infty r \exp(-10(r-1)^2 - \frac{1}{r}) dr$. For the diffusion, we obtain

$$\begin{aligned} \nabla_\xi^T a \nabla_\xi &= \left(\frac{\partial \xi}{\partial x} \right)^2 + \left(\frac{\partial \xi}{\partial y} \right)^2 \\ &= J(x, y) = \frac{1}{r^2}. \end{aligned}$$

Inserting this into Eq. (15) and using the same arguments as before, we end up with

$$a^\xi(\varphi) = \frac{C_1}{C_2}.$$

B. Galerkin Approximation for Deca Alanine

We apply TICA [51] to the the time series of 16 backbone dihedral angles of the peptide. According to the criterion of kinetic variance [52], the first seven TICs are retained, and the k -means algorithm is used to discretize this space into 500 states. The k -means cluster-centers are used as centers for a basis of 500 isotropic multivariate Gaussian functions with covariance matrix equal to 0.5 times the identity. The optimal linear approximations $\hat{\psi}_1, \hat{\psi}_2$ to the first two eigenfunctions of \mathcal{K}_τ projected on this basis are computed by the variational to conformational dynamics [34], completing the definition of ξ . Based on 100 k -means clusters in the seven-dimensional TICA space mentioned above, we build a Markov state model which serves as reference for implied timescales and equilibrium probabilities.